Quantum transport through $C_{48}N_{12}$ based atomic devices

Yan Xu, Jian Wang,[a] and Shijie Xu
Department of Physics, The Center of Theoretical and Computational Physics, The University of Hong Kong, Pokfulam Road, Hong Kong, China

(Received 6 July 2005; accepted 19 January 2006; published online 15 March 2006)

We report numerical calculations on the quantum transport through $C_{48}N_{12}$ based devices from first principles. We find that the transport properties are very sensitive to orientations of the molecules to the electrode. Different orientations can give rise to semiconducting to metallic behaviors. Our results show that the charge transfer which can be tuned by the gate voltage plays an important role in determining the transport properties. By varying the gate voltages, the transport properties can be changed from semiconducting to metallic behaviors and thereby magnifying effect can be achieved. © *2006 American Institute of Physics*. [DOI: 10.1063/1.2174879]

I. INTRODUCTION

Recently the research of C_{60} molecule has received increasing attention since the pioneering work of Kroto *et al.*[1] Due to the unique structural and electronic properties of fullerenes, they can be doped in several different ways: endohedral doping, substitutional doping, and exohedral doping. *Ab initio* analysis of transport through a scandium-nitrogen-doped C_{80} device shows that this endohedral doping can double the current compared with the bare C_{80} device.[2] Another type of doped fullerene, i.e., substitutional doping, can also be made where one or more carbon atoms of fullerene are substituted by other atoms. More recently, much attention has been paid to alternate nitrogen-doped compounds. From the growth of cross-linked nano-onions of C and N, it is found that there exist $C_{48}N_{12}$ molecules in the form of aza-fullerenes.[3] The existence of a novel $C_{48}N_{12}$ aza-fullerene has also been supported by the *ab initio* total energy calculation.[4–6] Since these molecules such as $C_{48}N_{12}$ have different band structures from that of the C_{60} molecule, it has attracted a lot of attention to investigate the structural, electronic, vibrational, optical as well as the magnetic properties of these molecules.[7–16] However, up to now, less attention has been paid to the transport properties through $C_{48}N_{12}$ molecule.[15,17] Indeed, the transport properties of single molecules have been studied experimentally through some form of metal-molecule-metal junctions where large molecules such as C_{60} or benzene-dithiol molecule are being used.[18–21] It is the purpose of this paper to give a detailed theoretical study of transport properties of the $C_{48}N_{12}$ based nanodevices using the *ab initio* method.[22] In particular, we investigate the *I-V* characteristics of Al(100)–$C_{48}N_{12}$–Al(100) systems.[23] For three different orientations of the $C_{48}N_{12}$ molecule relative to the Al(100) electrode, we obtain different *I-V* characteristics showing metallic and semiconducting behaviors. We find that the charge transfer during the formation of the molecular junction plays an important role in determining the transport properties. For different orientations of the $C_{48}N_{12}$ molecule, the charge transfer can be different. If charge transfer is such that the lowest unoccupied molecular orbital (LUMO) is completely empty, the Fermi level of the electrode is in the conductance gap, leading to a semiconducting behavior. On the other hand, a metallic behavior is obtained if the charge transfer aligns the Fermi level of the electrode with the partially occupied LUMO state. This mechanism of charge transfer doping has been used for current switching for C_{60} molecule.[24] Since the gate voltage can critically control the charge transfer, we also study the effect of the gate voltage on the charge transfer from the device electrodes to the central molecular region. We find that the gate voltage can be used for current switching.

The rest of the paper is organized as follows. In Sec. II, we briefly discuss the formulation we used in the calculation. In Sec. III, the detailed numerical results are presented along with some discussion. Finally, the summary is given in Sec. IV.

II. THEORETICAL FORMULATION

For $C_{48}N_{12}$ molecule with Al electrodes, the quantum transport problem is solved using the *ab initio* technique of Ref. 22 where density functional theory (DFT) is carried out within the nonequilibrium Green's function (NEGF) formalism.[25,26] We use an *s*, *p*, and *d* real space linear combination of atomic orbital (LCAO) basis set[22,27] and define the atomic core by standard nonlocal norm conserving pseudopotentia.[28] The density matrix of the device is constructed via NEGF and the semi-infinite leads provide real space potential boundary conditions for the Kohn-Sham (KS) potential of the device scattering region: this region consists of the molecule plus several layers of the metal leads. The KS potential includes contributions from Hartree, exchange, correlation, the atomic core, and any other external potentials. The NEGF-DFT iteration is numerically converged to 10^{-4} eV which we determine to be reasonable for our purpose. The NEGF-DFT formalism has several good features for our purpose:[22,27] (i) it constructs charge density under external bias potential using NEGF, thereby treats open device structures within the full self-consistent atomistic model of DFT; (ii) it treats atoms in the device and the leads at

[a]Electronic mail: jianwang@hkusub.hku.hk

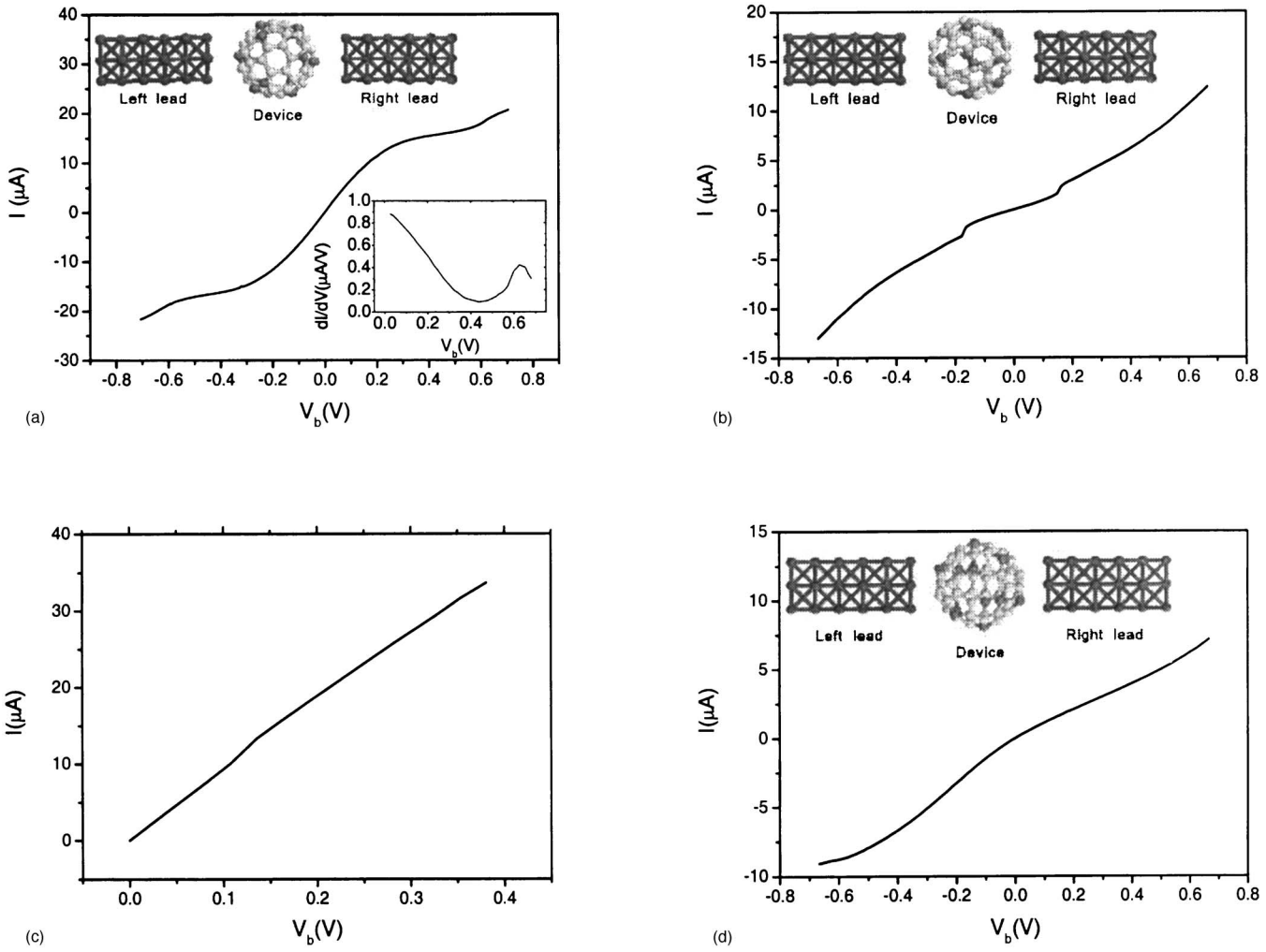

FIG. 1. The *I-V* characteristics of the Al(100)–$C_{48}N_{12}$–Al(100) at different orientations. (a) *I-V* curve of the first orientation. Left inset: Schematic plot of the first device. Right inset: dI/dV vs bias voltage. (b) *I-V* curve of the second orientation. Inset: Schematic plot of the second device. (c) *I-V* curve of the second orientation with a gate voltage V_g=13.6 eV applied in the central scattering region. (d) *I-V* curve of the third orientation. Inset: Schematic plot of the third device.

equal footing; (iii) it treats localized and scattering states at equal footing; and (iv) it is numerically efficient. The NEGF-DFT formalism[22,27] is now a standard tool for *ab initio* atomistic calculations of transport and we refer interested readers to the existing literature.[22,27] Here we only provide some details on the self-energy calculation of semi-infinite atomic electrode. The self-energy describes the coupling of the device scattering region to the two atomic electrodes and can be written in terms of the surface Green's function $\mathcal{H}_{\alpha\alpha}^{-1}$ (α=L, R). For instance,

$$\Sigma_{CC}^{L} = \mathcal{H}_{CL}\mathcal{H}_{LL}^{-1}\mathcal{H}_{LC}, \tag{1}$$

where the labels L, R, and C denote the regions of the left electrode, the right electrode, and the central simulation region. Here $\mathcal{H}_{\alpha\beta}=(H-ES)\alpha\beta$ (α, β=L, R, C) is a triblock diagonal matrix with H the Hamiltonian, E the energy, and S the overlap matrix for the atomic orbital basis set. Since we are using the atomic electrode instead of jellium electrode, the scattering wave function in the electrode is Bloch wave instead of plane wave. Hence we have calculated the surface Green's functions by extending[22] a technique discussed in Ref. 29.

III. RESULTS AND DISCUSSION

Using the first-principles calculation described above we now present the calculation of *I-V* characteristics of Al(100)–$C_{48}N_{12}$–Al(100) systems. For three different orientations of the $C_{48}N_{12}$ molecule [labeled as $C_{48}N_{12}(1)$, $C_{48}N_{12}(2)$, and $C_{48}N_{12}(3)$], we obtain different *I-V* characteristics showing metallic and semiconducting behaviors. We find that the charge transfer during the formation of the molecular junction plays an important role in determining the transport properties. We also study the effect of the gate voltage on the charge transfer from the device electrodes to the central molecular region. Our results show that the conductance of $C_{48}N_{12}$ junction is much smaller than that of the C_{60} system which can be understood from the charge transfer.

A. The first asymmetric configuration

In Fig. 1(a), we plot the *I-V* characteristics of the Al(100)–$C_{48}N_{12}(1)$–Al(100). We see that the *I-V* curve is lightly asymmetric about the bias voltage since the orientation of the $C_{48}N_{12}$ is such that it is asymmetric along the z direction [see left inset of Fig. 1(a)]. From Fig. 1(a) we see

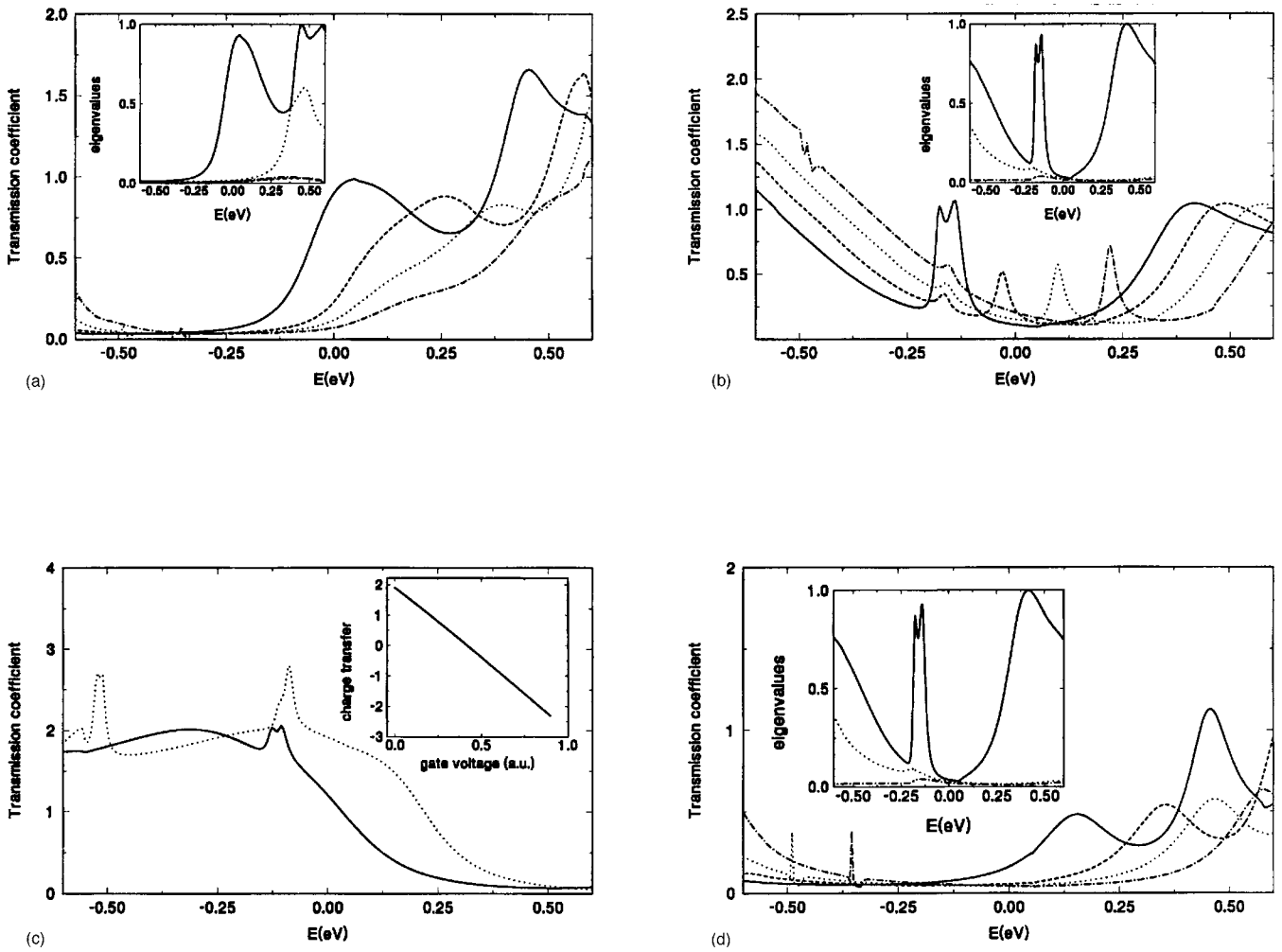

FIG. 2. The transmission coefficient $T(E,V_b)$ vs energy. (a) For the first orientation at different bias voltages: V_b=0.0 V (solid line), V_b=0.27 V (dashed line), V_b=0.41 V (dotted line), and V_b=0.54 V (dot-dashed line). Inset: Transmission eigenvalues as a function of electron energy at V_b=0. (b) For the second orientation at different bias voltages: V_b=0.0 V (solid line), V_b=0.14 V (dashed line), V_b=0.27 V (dotted line), and V_b=0.41 V (dot-dashed line). Inset: Transmission eigenvalues as a function of electron energy at V_b=0. (c) For the third orientation at different gate voltages: V_g=13.6 V (solid line) and V_g =21.8 V (dashed line). Inset: The charge transfer vs gate voltage. (d) For the third orientation at different bias voltages: V_b=0.0 V (solid line), V_b=0.27 V (dashed line), V_b=0.41 V (dotted line), and V_b=0.54 V (dot-dashed line). Inset: Transmission eigenvalues as a function of electron energy at V_b=0.

that, initially, the current increases quickly. At the bias voltage V_b=0.3 V the current starts to saturate and then increases again for V_b>0.6 V. The current is in the range of 20 μA at V_b=0.7 V which is much smaller than that (approximately 50 μA) of the corresponding Al(100)–C_{60}–Al(100) junction.[24] The differential conductance dI/dV versus bias voltage is shown in the right inset of Fig. 1(a). We see that at the Fermi level (when V_b=0), the conductance G is the largest showing metallic behavior with $G \sim e^2/h$. It decreases quickly, reaches the minimum at V_b=0.4 V, and increases after that. To understand the behavior of the *I-V* curve, we depict in Fig. 2(a) the transmission coefficient $T(E,V_b)$ versus energy E at different bias voltages.[30] We see that there are two peaks for the transmission coefficient at zero bias, one near the Fermi level and the other one is near E=0.44 eV. In the inset of Fig. 2(a), we have diagonalized the transmission matrix and found two eigenchannels[31] contributing to the current. As the bias voltage increases, the first peak in the transmission coefficient shifts toward the positive energy while the peak value decreases slightly. This shift is responsible for the decrease of dI/dV in the right inset of Fig. 1(a). Since the current is obtained by integrating $T(E,V_b)$ from 0 to V_b, the current increases as the bias voltage increases. To gain further insight, we study the charge transfer during the formation of the Al(100)–$C_{48}N_{12}$–Al(100) junction. For an isolated $C_{48}N_{12}$ molecule, there is a charge transfer from C to N since N dopes hole into the carbon system. Orbital energies E_K of the Kth eigenstate of an isolated $C_{48}N_{12}$ are shown in Fig. 3. Since there are 252 valence electrons, the highest occupied molecular orbital (HOMO) (doubly degenerate) of the molecule is completely filled with four electrons leaving the LUMO state (singly degenerate) empty. Hence, this molecule would be an insulator if we donot dope it. However, when the $C_{48}N_{12}$ molecule is connected to Al electrodes, further charge transfer occurs. In Fig. 4(a), we show the contour plot of the equilibrium charge density of Al(100)–$C_{48}N_{12}$(1)–Al(100) along the middle cross section (x=0) of the device at zero bias voltage. Note the perfect match across the boundaries between the molecular region and the electrode. The charge density of the electrodes is

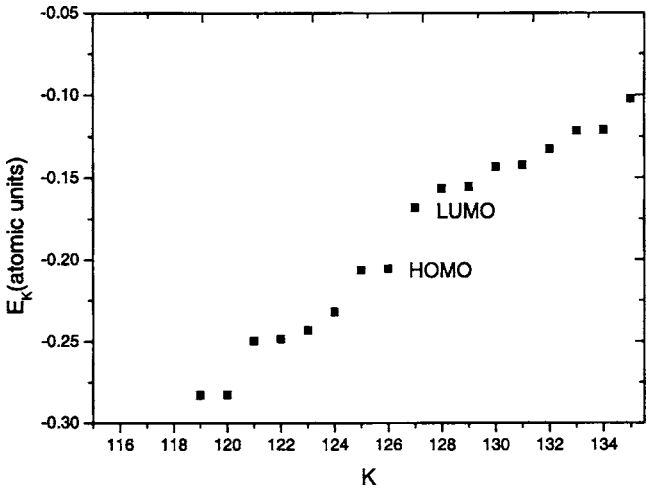

FIG. 3. Orbital energies E_K of the Kth eigenstate of an isolated $C_{48}N_{12}$.

affected by the molecule $C_{48}N_{12}$, but this effect is well screened away from the molecule. As a result we found that, in equilibrium, about 0.8 electron flows into the molecular region from the Al electrodes so that a common Fermi level is established. This extra charge transfer of 0.8 electron will make the LUMO state of the isolated $C_{48}N_{12}$ almost half filled, leading to a drastic enhancement of the conductance near the Fermi level. Therefore, the $Al(100)-C_{48}N_{12}(1)-Al(100)$ is metallic at zero bias.

B. The second symmetric configuration

Now we look at the second configuration by rotating the molecule $C_{48}N_{12}$ such that two parallel carbon hexagons are facing the Al electrodes [see the inset of Fig. 1(b)]. The I-V characteristics of the $Al(100)-C_{48}N_{12}(2)-Al(100)$ are depicted in Fig. 1(b). The I-V curve is symmetric about the bias voltage. The current is in the range of 14 μA at $V_b=0.7$ V which is much smaller than that of the first configuration. We also notice that the current jumps at about $V_b=0.16$ V. To understand this jump, we examine the transmission coefficient $T(E,V_b)$ versus energy [see Fig. 2(b)]. We see that in equilibrium ($V_b=0$) the transmission coefficient has a minimum at the Fermi level, giving rise to an insulating behavior which is very different from the first configuration. There are two peaks around $E=-0.15$ eV which are close together corresponding to two resonant states. From the eigenchannel analysis [the inset of Fig. 2(b)], we see that in the energy range $[-0.2,0.2]$ eV, the transport is dominated by a single eigenchannel. As we apply the bias voltage, one of the peaks in the transmission coefficient moves toward the positive energy. At around $V_b=0.16$ V, this peak moves across the Fermi level and contributes to the energy integral of the transmission coefficient, leading to a jump in the current. As the bias voltage increases further the current increases similar to the current before the jump. To confirm this insulating behavior in the equilibrium, in Fig. 4(b) we show the contour plot of the equilibrium charge density of the second configuration. From the figure, we see that more electrons have been transferred to the system. Indeed, we found that, in equilibrium, about electrons flow into the molecular region during the formation of the molecular junction. From Fig. 3, we conclude that the molecular LUMO state is completely filled when the molecule is connected to the Al electrodes, resulting to a semiconducting behavior with a much smaller conductance near the Fermi level, as shown in Fig. 2(b). Since the gate voltage V_g can critically control the charge transfer, which in turn determines the transport properties near the Fermi level, we plot in Fig. 1(c) the I-V curve versus the bias voltage when $V_g=13.6$ eV.[32] We see that the current varies almost linearly with the bias voltage. There is a tiny jump in the current near $V_b=0.14$ V. The physical origin of this jump is similar to the case without the gate voltage. In the presence of the gate voltage, the current increases about five times. This is due to the charge transfer which is shown in the inset of Fig. 2(c). In the presence of the gate voltage, charges have been depleted away from the molecule. We see from the inset of Fig. 2(c) that the charge transfer is a linear function of the gate voltage which agrees with previous calculation.[24] In the absence of the gate voltage, we have electrons transferred from the Al electrodes to the molecule so that LUMO state is filled. At $V_g=13.6$ V, the charge transfer is -0.5 electron instead of electrons. This means that about 2.5 electron charges are pulled back from the molecule to the Al electrodes. This makes the HOMO state of the isolated $C_{48}N_{12}$ partially empty which enhances the conductance at the Fermi level, resulting to a metallic behavior.[33] In the main panel of Fig. 2(c), we plot the transmission coefficient versus energy at two different gate voltages $V_g=13.6$ and 21.8 V. We see

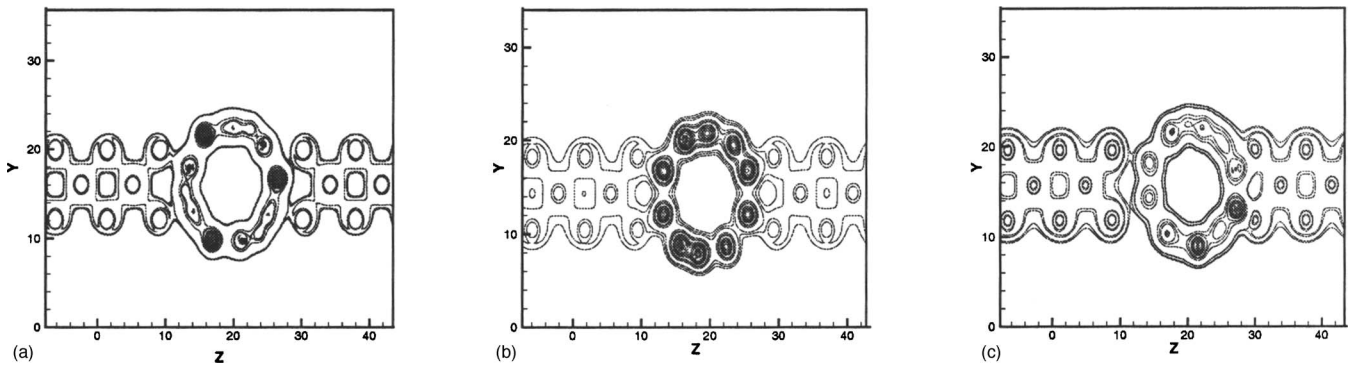

FIG. 4. Contour plot of the equilibrium charge density along the middle cross section of the device at zero bias voltage. (a) For the first orientation, (b) for the second orientation, and (c) for the third orientation.

that the conductance at Fermi level increases from 0.1 for $V_g=0$ to 1.2 for $V_g=13.6$ V. It increases further to 1.9 when $V_g=21.8$ V where the charge transfer is −2 electrons so that the HOMO state of the isolated $C_{48}N_{12}$ is half filled, leading to the maximum conductance. For the Al−C_{60}−Al molecular junction studied in Ref. 24, the HOMO state is half filled and the system is metallic in the absence of the gate voltage. When the gate voltage is applied, the HOMO state can be filled completely due to the charge transfer, giving rise to a semiconducting behavior. For our Al−$C_{48}N_{12}(2)$−Al molecular junction, it is the opposite case. The gate voltage can switch from a semiconducting state to a metallic state.

C. The third asymmetric configuration

Finally, we study the third configuration by rotating the $C_{48}N_{12}$ molecule such that two parallel hexagons, each contains one N atom, are facing the Al electrodes [see the inset of Fig. 1(d)]. The *I-V* curve is shown in Fig. 1(d). We see that the current is slightly asymmetric about the bias voltage due to the symmetry of the $C_{48}N_{12}$ molecule. The current is about 7 μA at $V_b=0.6$ eV which is much smaller than that of the other two configurations. In Fig. 2(d) we plot the transmission spectrum of the third configuration for different bias voltages. We see that at Fermi level $E=0$, $T(E,V_b=0)=0.16$, showing an insulating behavior similar to the second configuration. When the bias voltage is smaller than $V_b=0.15$ eV the currents of two configurations are about the same. The reason that the current of the third configuration is smaller than that of the second configuration after $V_b=0.15$ eV is due to the absence of the resonant states which are responsible for the jump in Fig. 1(b). In Fig. 4(c), we show the contour plot of the equilibrium charge density of the third configuration. In Table I, we list the coordinates of each atom in the $C_{48}N_{12}$ molecule with the corresponding excess charge in the presence of Al electrodes. The excess charge in the absence of electrodes can be found in Ref. 7. We found that, in equilibrium, about 1.9 electrons flow into the molecular region from Al electrodes. This gives rise to a filled molecular LUMO state and confirms the insulating behavior in equilibrium.

IV. SUMMARY

We have studied quantum transport through the $C_{48}N_{12}$ based molecular devices from first principles. Since it is very difficult to determine experimentally the orientation of the molecule relative to the electrodes, we have investigated the transport properties of the molecular device with different orientations. We found that the *I-V* curves depend critically on the orientation of the $C_{48}N_{12}$ molecule with respect to the Al electrodes. For three different orientations of the $C_{48}N_{12}$ molecule relative to the Al(100) electrode, we obtained different *I-V* characteristics showing metallic and semiconducting behaviors. We found that the charge transfer during the formation of the molecular junction plays an important role in determining the transport properties. For different orientations of the $C_{48}N_{12}$ molecule, the charge transfer can be different. If the charge transfer is such that the lowest unoccupied molecular orbital (LUMO) is completely empty, the

TABLE I. The excess charge distribution Q of $C_{48}N_{12}$.

Atom	Coordinates	Q
C	(17.65,14.72,8.84)	0.20
C	(16.67,10.39,19.56)	0.02
C	(16.09,12.56,21.16)	0.14
C	(10.37,11.48,18.00)	−0.09
C	(13.09,9.42,12.00)	−0.10
C	(20.37,12.75,18.00)	−0.09
C	(9.07,12.34,13.93)	−0.11
C	(13.92,17.44,21.15)	0.02
C	(16.58,17.16,21.16)	0.11
N	(17.34,10.50,10.18)	0.31
C	(18.16,18.75,19.56)	0.02
C	(9.88,12.73,11.38)	−0.10
C	(16.08,12.56,8.85)	0.02
C	(14.27,20.77,18.00)	−0.09
C	(12.34,15.29,8.85)	0.07
C	(20.93,17.66,16.07)	−0.11
C	(16.57,17.16,8.85)	−0.02
C	(11.12,19.44,12.00)	−0.11
C	(19.71,19.47,14.55)	−0.10
C	(15.66,21.46,13.93)	−0.10
C	(14.40,9.43,18.63)	−0.10
C	(14.34,8.54,16.07)	−0.10
C	(16.51,8.69,14.55)	−0.10
C	(18.88,10.56,18.00)	−0.11
C	(10.29,10.53,15.45)	−0.10
N	(18.94,9.43,15.52)	0.32
N	(8.21,14.38,15.52)	0.32
C	(21.23,13.15,15.44)	−0.10
N	(20.08,14.78,19.81)	0.31
C	(10.48,18.30,18.63)	−0.11
C	(20.13,17.27,18.62)	−0.10
C	(13.42,12.84,8.84)	0.11
C	(19.52,11.70,11.37)	−0.11
C	(9.74,18.80,16.07)	−0.10
N	(9.92,15.22,10.19)	0.32
C	(19.82,14.14,10.44)	0.02
N	(17.86,21.19,15.52)	0.32
N	(11.06,20.57,14.48)	0.32
C	(13.33,19.61,10.44)	0.02
C	(15.60,20.57,11.37)	−0.10
N	(12.28,10.71,19.82)	0.31
C	(13.43,12.84,21.15)	−0.02
N	(12.14,8.81,14.48)	0.32
C	(15.73,9.23,12.00)	−0.09
C	(9.22,13.86,18.01)	−0.11
C	(17.66,14.71,21.15)	0.07
C	(10.18,15.86,19.56)	0.02
C	(20.26,11.20,13.93)	−0.10
C	(11.84,11.25,10.44)	0.02
N	(12.66,19.50,19.82)	0.31
C	(8.77,16.84,14.56)	−0.10
N	(21.79,15.62,14.48)	0.32
C	(16.91,20.58,18.00)	−0.10
C	(9.63,17.25,12.00)	−0.09
C	(20.78,16.14,11.99)	−0.11
C	(13.91,17.44,8.84)	0.14
C	(13.49,21.31,15.45)	−0.10
C	(19.63,18.52,12.00)	−0.09
N	(17.72,19.29,10.18)	0.31
C	(12.35,15.28,21.16)	0.20

Fermi level of the electrode is in the conductance gap, leading to a semiconducting behavior. On the other hand, a metallic behavior is obtained if the charge transfer aligns the Fermi level of the electrode with the partially occupied LUMO state. Since the gate voltage can critically control the charge transfer, we have also studied the effect of the gate voltage on the charge transfer from the device electrodes to the central molecular region. We found that the gate voltage can be used for current switching. For a particular orientation of the $C_{48}N_{12}$ molecule (the second configuration in our study), its transport behavior can be changed from insulating to metallic by the gate voltage $V_g=21.8$ eV. For the gate voltage $V_g=13.6$ eV, the current can be magnified by five times than that of $V_g=0$.

ACKNOWLEDGMENTS

We thank Professor H. Guo for providing the coordinates of $C_{48}N_{12}$ and many useful discussions. We gratefully acknowledge support by a RGC grant from the SAR Government of Hong Kong under Grant No. HKU 7032/03P and a grant from CRCG of The University of Hong Kong.

[1] H. Kroto, J. R. Heath, S. C. O'Brian, R. F. Curl, and R. E. Smalley, Nature (London) **318**, 162 (1985).
[2] B. Larade, J. Taylor, Q. R. Zheng, H. Mehrez, P. Pomorski, and H. Guo, Phys. Rev. B **64**, 195402 (2001).
[3] L. Hultman, S. Stafström, Z. Czigány, J. Neidhardt, N. Hellgren, I. F. Brunell, K. Suenaga, and C. Cooliex, Phys. Rev. Lett. **87**, 225503 (2001).
[4] S. Stafström, L. Hultman, and N. Hellgren, Chem. Phys. Lett. **340**, 227 (2001).
[5] D. Schultz, R. Droppa, Jr., F. Alvarez, and M. C. dos Santos, Phys. Rev. Lett. **90**, 015501 (2003).
[6] M. R. Manaa, H. A. Ichord, and D. W. Sprehn, Chem. Phys. Lett. **378**, 449 (2003).
[7] R. H. Xie, G. W. Bryant, and V. H. Smith, Jr., Chem. Phys. Lett. **368**, 486 (2003).
[8] M. R. Manaa, H. A. Ichord, and D. W. Sprehn, Chem. Phys. Lett. **378**, 449 (2003).
[9] R. H. Xie, G. W. Bryant, and V. H. Smith, Jr., Phys. Rev. B **67**, 155404 (2003).
[10] M. R. Manaa, Chem. Phys. Lett. **382**, 194 (2003).
[11] H. Liu and J. W. Chen, Phys. Status Solidi B **237**, 575 (2003).
[12] B. Brena and Y. Luo, J. Chem. Phys. **119**, 7139 (2003).
[13] R. H. Xie, L. Jensen, G. W. Bryant, J. J. Zhao, and V. H. Smith, Jr., Chem. Phys. Lett. **375**, 445 (2003).
[14] B. Schimmelpfennig, H. Agren, and S. Csillag, Synth. Met. **132**, 265 (2003).
[15] R. G. Viglione and R. Zanasi, Phys. Chem. Chem. Phys. **6**, 295 (2004).
[16] M. R. Manaa, Solid State Commun. **129**, 379 (2004).
[17] R. H. Xie, G. W. Bryant, J. J. Zhao, V. H. Smith, Jr., A. D. Carlo, and A. Pecchia, Phys. Rev. Lett. **90**, 206602 (2003).
[18] C. Joachim, J. K. Gimzewski, P. R. Schlittler, and C. Chavy, Phys. Rev. Lett. **74**, 2102 (1995).
[19] J. L. Segura and N. Martin, Chem. Soc. Rev. **29**, 13 (2000).
[20] H. Park, J. Park, A. K. L. Lim, E. H. Anderson, A. P. Alivisatos, and P. L. McEuen, Nature (London) **407**, 57 (2000).
[21] B. Q. Xu and N. J. Tao, Science **301**, 1221 (2003).
[22] J. Taylor, H. Guo, and J. Wang, Phys. Rev. B **63**, 245407 (2001).
[23] The experiments are usually done for Au electrodes rather than the Al electrodes. For Au atoms, it requires 11 orbitals and the convergence is much slower. Due to the computational limitation, we only study the Al electrode. It would be interesting to compare the results for Au electrode and Al electrode.
[24] J. Taylor, H. Guo, and J. Wang, Phys. Rev. B **63**, 121104 (2001).
[25] A. P. Jauho, N. S. Wingreen, and Y. Meir, Phys. Rev. B **50**, 5528 (1994).
[26] B. G. Wang, J. Wang, and H. Guo, Phys. Rev. Lett. **82**, 398 (1999).
[27] M. Brandbyge, J.-L. Mozos, P. Ordejón, J. Taylor, and K. Stokbro, Phys. Rev. B **65**, 165401 (2002).
[28] D. R. Hamann, M. Schlüter, and C. Chiang, Phys. Rev. Lett. **43**, 1494 (1982).
[29] S. Sanvito, C. J. Lambert, J. H. Jefferson, and A. M. Bratkovsky, Phys. Rev. B **59**, 11936 (1999).
[30] We have shifted the origin of the energy such that the Fermi level corresponds to $E=0$.
[31] M. Brandbyge, M. R. Sorenson, and K. W. Jacobsen, Phys. Rev. B **56**, 14956 (1997).
[32] The reason that one has to apply a large gate voltage to affect the charge transfer is because the metallic electrodes absorb most of the electric field lines so that the effective gate voltage experienced by the molecular region is much smaller.
[33] B. Larade, J. Taylor, H. Mehrez, and H. Guo, Phys. Rev. B **64**, 075420 (2001).